Original Article

Interocular asymmetry of choroidal thickness and vascularity index measurements in normal eyes assessed by swept-source optical coherence tomography

Jie Lu[1], Hao Zhou[1], Yingying Shi[2], James Choe[1], Mengxi Shen[2], Liang Wang[2], Kelly Chen[1], Qinqin Zhang[1], William J. Feuer[2], Giovanni Gregori[2], Philip J. Rosenfeld[2], Ruikang K. Wang[1,3]^

[1]Department of Bioengineering, University of Washington, Seattle, WA, USA; [2]Department of Ophthalmology, Bascom Palmer Eye Institute, University of Miami Miller School of Medicine, Miami, FL, USA; [3]Department of Ophthalmology, University of Washington, Seattle, WA, USA

Contributions: (I) Conception and design: PJ Rosenfeld, RK Wang; (II) Administrative support: J Lu, Y Shi, PJ Rosenfeld, RK Wang; (III) Provision of study materials or patients: Y Shi, M Shen, L Wang; (IV) Collection and assembly of data: Y Shi, M Shen, L Wang; (V) Data analysis and interpretation: J Lu, H Zhou, Y Shi, J Choe, WJ Feuer, G Gregori, PJ Rosenfeld; (VI) Manuscript writing: All authors; (VII) Final approval of manuscript: All authors.

Correspondence to: Ruikang K. Wang. University of Washington, Box 355061, 3720 15th Ave NE, Seattle, WA 98195-5061, USA.
Email: wangrk@uw.edu.

Background: To investigate the symmetry of interocular choroidal thickness and vascularity index measurements in normal eyes using swept-source optical coherence tomography (SS-OCT). Cross-sectional and observational study. This study included 244 eyes of 122 normal adults with ages uniformly distributed from 19 to 89 years.

Methods: SS-OCT imaging was performed using a scanning pattern of 12×12 mm. Mean choroidal thickness (MCT) and choroidal vascularity index (CVI) measurements in the entire scanning region were obtained using a validated and published automatic method. The correlation and differences (including signed and absolute differences) between bilateral MCT and CVI measurements were analyzed at the following 6 regions: 3 concentric circles centered on the fovea with diameters of 2.5, 5, and 11 mm; the inner rim from 2.5 to 5 mm circle; the outer rim from 5 to 11 mm circle; and the entire 12×12-mm scan region, respectively. Comparison of interocular MCT and CVI measurements.

Results: MCT measurements in right and left eyes were strongly correlated in all regions [all intraclass correlation (ICC) >0.73], but MCT measurements in right eyes were significantly thicker than in left eyes. CVI measurements in right and left eyes were moderately correlated in all regions (all ICC >0.46), but CVI measurements in right eyes were significantly smaller than that in left eyes in the macular subregions (2.5 mm circle, 5 mm circle, and the inner rim). Neither signed nor absolute interocular differences in MCT were correlated with corresponding CVI interocular differences.

Conclusions: Choroidal differences exist between normal fellow eyes in adults in the absence of obvious pathology. This study is useful in assisting clinicians and researchers in distinguishing asymmetric changes that are to be expected in normal eyes versus changes that could be associated with diseases.

Keywords: Optical coherence tomography (OCT); choroidal thickness; choroidal vascularity index (CVI); interocular asymmetry; normative range

Submitted Aug 16, 2021. Accepted for publication Aug 25, 2021.
doi: 10.21037/qims-21-813
View this article at: https://dx.doi.org/10.21037/qims-21-813

^ ORCID: 0000-0001-5169-8822.

Introduction

Identifying asymmetrical or unilateral features between fellow eyes is important in the investigations of ocular diseases that only affect one eye or are initiated unilaterally but eventually progress bilaterally. It is important to establish a baseline of interocular asymmetry in normal eyes that can be used to assist clinicians and researchers in differentiating pathological differences from physiological asymmetries. Previous studies have demonstrated that some degrees of non-pathologic asymmetry can exist in the retina and choroid between fellow eyes using optical coherence tomography (OCT) (1-8).

OCT is a well-established non-invasive imaging method with high resolution that can be performed in real-time and provides three-dimensional (3D) imaging capabilities. Recent advances in swept-source OCT (SS-OCT) development make it an ideal tool for choroidal imaging because of its deeper penetration depth enabled by longer wavelength, faster imaging speed and negligible sensitivity roll-off (9). When investigating the choroidal symmetry in children (10) and young adults (11-13), a number of groups utilized spectral-domain OCT (SD-OCT) with enhanced depth imaging (EDI) (14). However, SD-OCT is limited by its depth of penetration, leading to relatively poor imaging quality in the choroidal layer. While EDI improves the quality of choroidal imaging, it only improves depth imaging within the macula and is difficult to perform a wide field-of-view (FOV) imaging (14). In addition, most of the participants of the above studies were less than 50 years old, which provides limited understanding of the choroidal symmetry within the elderly population. Although SS-OCT has been used to investigate interocular symmetry of the choroidal thickness in adults with normal eyes (8,15), the results were derived by using manual measurements from several selected B-scans, which is time consuming and augments the possibilities of subjective bias.

Recently, attention has been paid to mapping the choroidal thickness and choroidal vascularity index (CVI) measurements from the entire 12×12 mm scan that encompasses a 40-degree FOV centered on the fovea. In prior work, we have generated a normative age-dependent database of choroidal thickness and CVI measurements using the SS-OCT 12×12 mm datasets (16). However, we did not study the extent of interocular symmetry in these eyes over the entire scanning region.

The purpose of this study is to use widefield SS-OCT imaging to assess whether physiological choroidal asymmetry exists between fellow normal eyes within the entire SS-OCT 12×12 mm scan regions. The extent of physiological choroidal symmetry was assessed by comparing the mean choroidal thickness (MCT) and CVI measurements between the two normal eyes. We present the following article in accordance with the STROBE reporting checklist (available at https://dx.doi.org/10.21037/qims-21-813).

Methods

Study participants

This was a cross-sectional study of SS-OCT choroidal imaging in normal adults with ages uniformly distributed from 19 to 89 years. This study was approved by the Institutional Review Board (IRB) of Medical Sciences Subcommittee at the University of Miami, Miller School of Medicine and was conducted in compliance with the Declaration of Helsinki (as revised in 2013). All the participants had a normal ocular history in both eyes. Study exclusion criteria included: (I) visual complaints; (II) retinal, optic nerve or choroidal pathologies detected on examination or with OCT imaging; (III) diabetes history; (IV) uncontrolled hypertension. The sample size was determined by the number of participants who met our inclusion criteria during the study period. All participants voluntarily gave written informed consents before scans were taken.

OCT imaging and axial length measurements

OCT scanning was performed using a commercial SS-OCT instrument (PLEX® Elite 9000, Carl Zeiss Meditec, Dublin, CA, USA). This instrument was equipped with a 100 kHz swept laser source with a central wavelength of 1,050 nm and a spectral bandwidth of 100 nm, providing an axial resolution of ~5 μm in tissue. Each OCT scan centered on the fovea covered a FOV of 12×12 mm with a lateral resolution of ~20 μm, and a measured depth of 3.0 mm (1,536 pixels) in tissue. The OCT angiographic scan pattern consisted of 500 A-lines per 6 mm horizontal B-scan, 500 B-scan positions along the vertical scanning dimension, and two repeated B-scans per B-scan positions. A non-contact biometry instrument was used to measure axial length (IOLMaster, Carl Zeiss Meditec). Eyes were excluded from the study if their axial length was more than 26 mm, and OCT scans were excluded from this study if there were

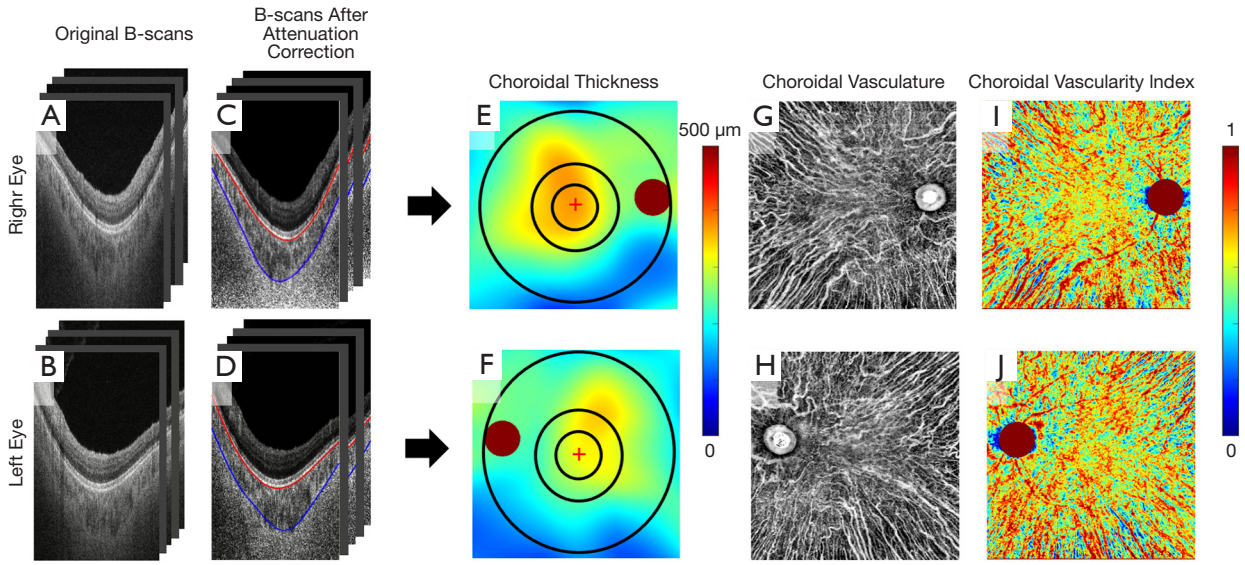

Figure 1 Cross-sectional B-scan and *en face* choroidal images taken of a 63-year-old woman. (A,B) Original cross-sectional B-scans. (C,D) Cross-sectional B-scans after attenuation correction. Red lines highlight the upper boundary of the choroid (i.e., Bruch's membrane), and blue lines highlight the bottom boundary of the choroid (i.e., choroid-sclera interface). (E,F) Overlay of three concentric circles centered on the fovea on the choroidal thickness maps. These circles divide the 12×12 mm scan into 6 regions for quantification: the 2.5 mm circle, 5 mm circle, 11 mm circle, inner rim (from the 2.5 mm circle to the 5 mm circle), outer rim (from the 5 mm circle to the 11 mm circle), and the entire 12×12 mm scan. +: fovea. Color bar represents a depth range of 0–500 µm. (G,H) *En face* choroidal vasculature maps. (I,J) *En face* choroidal vascularity index maps. Color bar represents a value range of 0–1.

noticeable motion artifacts or signal strength was less than 7 (recommended by the manufacturer). All imaging scans and biometric measurements were performed by trained operators at the department of ophthalmology, Bascom palmer eye institute, Miami, FL, USA.

Choroidal segmentation

The choroidal slab was acquired by automatically outlining the choroidal boundaries (i.e., Bruch's membrane and choroid-sclera interface) using a validated algorithm (17). The contrast of the choroid-sclera interface [here referred to as the outer border of choroidal vessels (18)] was relatively low in the original OCT images because the intensity of OCT light is exponentially attenuated along its path as the light beam propagates through the highly scattering RPE complex and choroid (*Figure 1A,1B*). To enhance the contrast of the choroid-sclera interface in the OCT image, the algorithm applied an attenuation correction strategy consisting of attenuation compensation and exponentiation to the structural images (17,19) (*Figure 1C,1D*). Optic discs were excluded from the volumetric datasets before choroidal segmentation. The choroidal boundaries were then automatically detected through the graph search method (*Figure 1C,1D*). Even though previous studies have shown excellent agreement between this automatic method and manual segmentation (16,17). We still manually checked the automatic segmentation for accuracy once completed.

MCT measurements

The distance between the Bruch's membrane and choroid-sclera interface was used to generate *en face* choroidal thickness maps (*Figure 1E,1F*), where the color represented a thickness range between 0–500 µm. On each *en face* map, three concentric circles centered on the fovea with diameters of 2.5, 5, and 11 mm, respectively, were created to generate 6 regions for quantification: the 2.5 mm circle, 5 mm circle, 11 mm circle, inner rim (from 2.5 to 5 mm circle), outer rim (from 5 to 11 mm circle), and the entire 12×12 mm scan (*Figure 1E,1F*). The foveal location was automatically detected through searching the local minimum thickness of the retinal layers in OCT structural

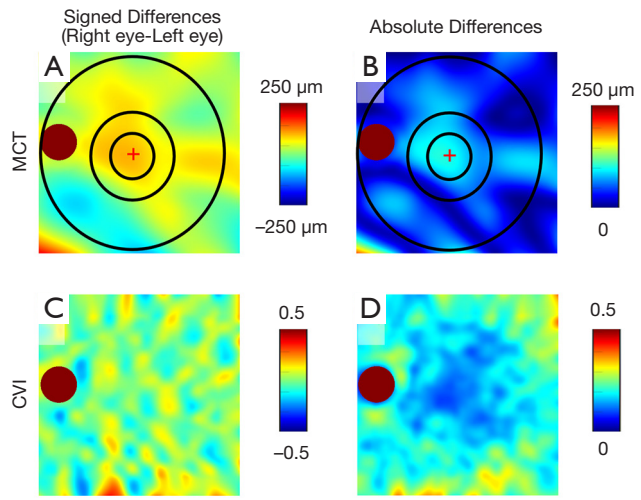

Figure 2 *En face* images of interocular choroidal differences. (A) Signed interocular differences in MCT. Color bar represents a depth range of –250 to 250 μm. (B) Absolute interocular differences in MCT. Color bar represents a depth range of 0 to 250 μm. (C) Signed interocular differences in the choroidal vascularity index (CVI). Color bar represents a value range of –0.5 to 0.5. (D) Absolute interocular differences in CVI. Color bar represents a value range of 0 to 0.5. MCT, mean choroidal thickness; CVI, choroidal vascularity index.

images. In this study, we used the MCT (referred to as the average value of the thickness within a region of interest) to represent the regional choroidal thickness (excluding the optic disc).

CVI measurements

Figure 1C,1D show B-scans with dark vascular structures within the choroidal layer. These structures are thought to be choroidal vessels because most of the light is scattered forward by the blood, allowing the large choroidal vessels to appear as dark regions (low backscattered light) with vessel-like shapes in the OCT images (20,21). In addition, the highly backscattering RPE significantly reduced the signal generated by the light that was backscattered by the choroidal vasculature. Therefore, it is difficult for conventional OCT angiography (OCTA) methods (22) to detect the choroidal blood flow signal (20,21). In this study, the choroidal vessels were obtained from the OCT structural images after attenuation correction by segmenting dark regions with the vessel-like shapes in the choroid using Otsu's method (16,17,23). For convenient visualization, we inverted the dark regions to appear bright (*Figure 1G,1H*). The CVI was estimated by dividing the number of pixels in the choroidal vessels by the total number of pixels in the choroidal slab. The *en face* CVI map was generated by mapping the CVI value at each A-line (*Figure 1I,1J*), where the color represents a CVI value range of 0–1. For comparison, the 12×12 mm scan of the CVI was also divided by using the concentric circles mentioned above.

Interocular asymmetry measurements

The interocular asymmetry in the MCT and CVI measurements was quantified by using signed difference and absolute difference. The signed difference was calculated by subtracting the left eye value from the right eye value. To visualize interocular asymmetry, we flipped the right eye *en face* images in the left-right direction, registered the two images at fovea and optic nerve head, and then generated *en face* maps of interocular difference (*Figure 2*).

Statistical analysis

The data with normal distributions (e.g., MCT, CVI and signed interocular difference) were presented as the mean and standard deviation (SD), while the data without normal distribution (e.g., absolute interocular difference) were presented as the mean, SD, median and range. The strengths of correlations in corresponding regions of measurements between fellow eyes were analyzed by intraclass correlations (ICCs). ICCs >0.75 can be interpreted as strong or excellent, ICCs <0.3 are weak or poor, while intermediate ICCs are considered fair to good or moderate (24). Paired-sample *t*-tests were utilized to compare the measurements between fellow eyes.

The relationships between interocular differences in the MCT and CVI measurements were analyzed by using Pearson's correlation. Furthermore, the relationships between the interocular differences in MCT and CVI measurements and each of the variables: (I) participants' age, (II) interocular differences of axial length, were studied by Pearson's correlation. Statistical analysis was carried out using MATLAB R2020b and IBM SPSS V25 (Armonk, NY, USA), and scatter plots were generated using GraphPad Prism (GraphPad Software, San Diego, CA, USA). Statistical significance is represented at two levels: *, $P \leq 0.05$, **, $P \leq 0.01$.

Table 1 Demographic characteristics of the participants in this study

Characteristic	Total	Age decades						
		19–29	30–39	40–49	50–59	60–69	70–79	80–89
Number of patients [number of eyes]	122 [244]	14 [28]	19 [38]	15 [30]	18 [36]	22 [44]	18 [36]	16 [32]
Age (mean ± SD, years)	55.14±19.38	24.57±2.79	33.26±2.54	45.13±3.16	55.52±2.81	63.99±2.94	74.11±2.81	83.25±2.70
Gender (male/female)	49/73	7/7	11/8	4/11	2/16	10/12	8/10	7/9
Axial length (mean ± SD, mm)								
Right eye	23.84±0.89	24.43±1.07	24.01±0.81	24.13±0.83	23.69±1.04	23.87±0.78	23.39±0.79	23.47±0.63
Left eye	23.83±0.89	24.35±0.98	23.97±0.84	24.02±0.87	23.73±1.09	23.85±0.77	23.36±0.84	23.60±0.63

Results

A total of 254 normal eyes from 127 participants ranging from 19 to 89 years of age were enrolled in this study. Five participants were later excluded: two because their axial lengths were greater than 26 mm, one because the entire choroidal layer was beyond the A-scan range, and two because they were uncooperative, could not fixate, and the scans could not be adequately obtained. The final analysis included 122 participants (244 eyes), 49 men and 73 women, with a mean age of 55.14±19.38 years. The demographic characteristics of the participants are shown in *Table 1*. No significant differences were observed when comparing axial length between fellow eyes.

Figure 1 shows the choroidal thickness, choroidal vascularity, and the CVI maps derived from a 63-year-old participant. On visual inspection, the *en face* choroidal thickness and CVI maps did not appear completely symmetrical. The choroidal thickness in the right eye appeared thicker than that in the left eye in the macular (5 mm circle) region. For CVI maps, a homogeneously distributed mix of red to blue colors can be seen in both eyes; however, subtle differences can also be observed between the two eyes. *Figure 2* shows the interocular asymmetry maps derived from the same participant represented in *Figure 1*. The uneven appearance of the interocular asymmetry maps confirms the interocular choroidal differences shown in *Figure 1*. This participant demonstrated a thicker choroidal thickness in the 2.5 mm circle region in the right eye compared with that of the left eye (*Figure 2A*). The MCT absolute difference between fellow eyes in the 2.5 mm circle region is the most obvious difference in the entire scanning region (*Figure 2B*). Similarly, the CVI interocular asymmetry maps of this participant also showed varied differences across the entire scanned region between fellow eyes (*Figure 2C*,*2D*).

MCT and CVI measurements

The values, correlation coefficients, and comparisons of the bilateral measurements in MCT and CVI measurements are summarized in *Table 2*. MCT in the 5-mm circle region measured 261.75±80.67 μm in right eyes and 251.22±69.11 μm in left eyes. CVI in the 5 mm circle region was 0.618±0.024 in right eyes and 0.625±0.029 in left eyes. In all the regions, there was a strong correlation between fellow eyes in MCT, whereas there was only a moderate correlation between fellow eyes in CVI. MCT was statistically thicker in the right eyes than that in the left eyes in all the quantified regions. In contrast, CVI was statistically lower in the right eyes than that in the left eyes in the 2.5 mm circle, 5 mm circle, and inner rim regions. *Figure 3* shows the correlation and Bland-Altman agreement analysis on MCT and CVI measurements in the 5 mm circle region between fellow eyes.

Signed and absolute interocular differences in MCT and CVI measurements are summarized in *Tables 3*,*4*. The normal 95% limits of signed differences and absolute differences in MCT and CVI measurements could be used as a reference for physiological asymmetry. For example, if the MCT of the left eye is more than 77.75 μm thicker than the MCT of the right eye, or the MCT of the right eye is more than 125.71 μm thicker than the MCT of the left eyes in the 5 mm circle region, then this patient's interocular difference is thought to be abnormal. Alternatively, if the absolute interocular MCT difference is greater than 104.25 μm in the 5 mm circle region, then this patient's eyes are also considered abnormal. In addition,

Table 2 MCT and CVI measurements

Region quantified	MCT (n=122)				CVI (n=122)			
	Right eye (μm), mean (SD)	Left eye (μm), mean (SD)	Interocular intraclass correlation coefficient	P value of paired *t*-test	Right eye, mean (SD)	Left eye, mean (SD)	Interocular intraclass correlation coefficient	P value of paired *t*-test
2.5 mm circle	274.09 (95.47)	260.03 (74.91)	0.735	0.013*	0.618 (0.037)	0.627 (0.041)	0.462	0.018*
5 mm circle	261.75 (80.67)	251.22 (69.11)	0.812	0.011*	0.618 (0.024)	0.625 (0.029)	0.521	0.002**
Inner rim	257.42 (77.80)	246.99 (67.21)	0.812	0.010**	0.618 (0.024)	0.625 (0.029)	0.597	0.004**
11 mm circle	235.33 (60.70)	229.47 (59.07)	0.918	0.007**	0.607 (0.020)	0.610 (0.025)	0.520	0.079
Outer rim	226.57 (54.83)	222.32 (56.27)	0.919	0.035*	0.603 (0.021)	0.605 (0.025)	0.598	0.311
12×12	227.26 (54.41)	221.62 (53.89)	0.918	0.004**	0.609 (0.019)	0.612 (0.024)	0.599	0.091

*, P<0.05; **, P<0.01. MCT, mean choroidal thickness; CVI, choroidal vascularity index.

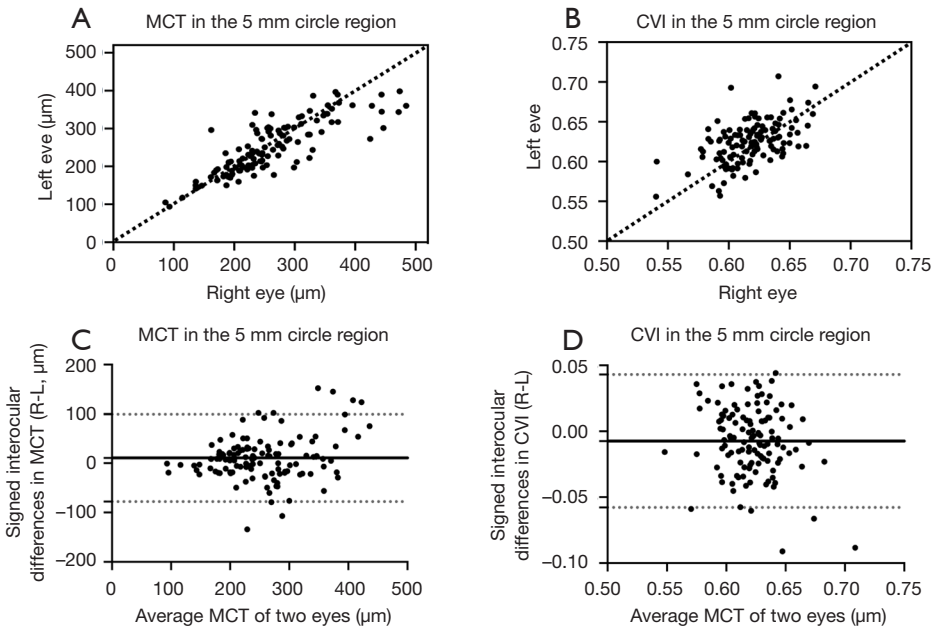

Figure 3 Correlation and Bland-Altman agreement analysis on MCT and CVI measurements in the 5 mm circle (macular) region between fellow eyes. The slope of the dashed lines in the correlation analysis maps (A,B) is 1. The solid lines in Bland-Altman agreement analyses (C,D) represent the bias, and the perforated lines represent the upper and lower 95% limits of agreement. MCT, mean choroidal thickness; CVI, choroidal vascularity index.

the box plots of signed interocular differences in MCT and CVI measurements are shown in *Figures 4,5*, respectively. *Figure 4* shows trends for right eyes to have thicker MCTs than left eyes in all the regions. Comparatively, *Figure 5* shows trends for right eyes to have lower CVIs in all the regions. Although a weak inverse relationship between signed interocular differences of MCT and signed interocular differences of CVI was observed in the 2.5-mm circle (Pearson's r=–0.21, P=0.020), the strength of the relationship was too weak to consider noteworthy (*Table 5*). Therefore, neither signed nor absolute interocular differences in MCT were correlated with corresponding CVI interocular differences in all the regions quantified (*Table 5* and *Figure 6*).

Table 3 Signed and absolute interocular differences in MCT

Region quantified	Signed interocular differences (right eye - left eye, μm)		Size of signed interocular differences (the average signed interocular differences as a percentage of the MCT, %)	Absolute interocular differences (μm)		
	Mean (SD)	Normal 95% limits (2.5% to 97.5% title)		Mean (SD)	Median (min, max)	Normal 95% limits (95% tile)
2.5 mm circle	14.06 (61.52)	−88.43 to 168.63	5.26	42.81 (46.22)	30.60 (1.55, 251.41)	139.89
5 mm circle	10.53 (45.21)	−77.75 to 125.71	4.11	33.17 (32.34)	20.99 (0.07, 152.04)	104.25
Inner rim	10.42 (43.74)	−77.78 to 109.08	4.13	32.33 (31.13)	19.64 (0.27, 148.08)	102.04
11 mm circle	5.86 (23.63)	−41.07 to 54.54	2.52	18.82 (15.36)	14.43 (0.08, 64.62)	52.33
Outer rim	4.25 (22.00)	−33.90 to 51.94	1.89	17.36 (14.09)	12.03 (0.34, 55.27)	47.65
12×12	5.64 (21.31)	−36.02 to 46.38	2.51	17.42 (13.42)	14.69 (0.21, 54.53)	44.48

MCT, mean choroidal thickness.

Table 4 Signed and absolute interocular differences in CVI

Region quantified	Relative interocular differences (right eye - left eye)		Size of signed interocular differences (the average signed interocular difference as a percentage of the average CVI, %)	Absolute interocular differences		
	Mean (SD)	Normal 95% limits (2.5% to 97.5% title)		Mean (SD)	Median (min, max)	Normal 95% limits (95% tile)
2.5 mm circle	−0.0087 (0.040)	−0.088 to 0.071	−1.40	0.0323 (0.0249)	0.0315 (0.0001, 0.1100)	0.074
5 mm circle	−0.0074 (0.0257)	−0.063 to 0.037	−1.19	0.0210 (0.0166)	0.0168 (0.0002, 0.0910)	0.050
Inner rim	−0.0067 (0.0256)	−0.070 to 0.034	−1.08	0.0199 (0.0173)	0.0159 (0.0001, 0.0919)	0.051
11 mm circle	−0.0032 (0.0201)	−0.046 to 0.035	−0.53	0.0158 (0.0128)	0.0141 (0.0001, 0.0604)	0.038
Outer rim	−0.0019 (0.0207)	−0.046 to 0.040	−0.32	0.0162 (0.0130)	0.0119 (0.0003, 0.0527)	0.042
12×12	−0.0030 (0.0196)	−0.044 to 0.036	−0.49	0.0155 (0.0122)	0.0131 (0.0003, 0.0579)	0.039

CVI, choroidal vascularity index.

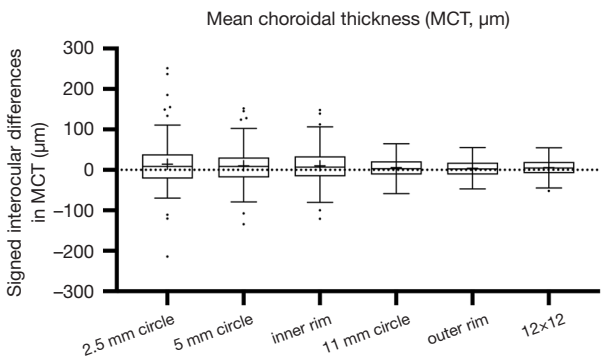

Figure 4 Tukey boxplots of the signed interocular difference of MCT from all 122 participants. Boxplots show the mean as "+". The perforated line indicates the zero. Trends for right eyes have thicker MCTs (the mean value larger than 0) shown in the 2.5 mm circle, 5 mm circle, inner rim, 11 mm circle, outer rim and entire 12×12 mm scan regions. MCT, mean choroidal thickness.

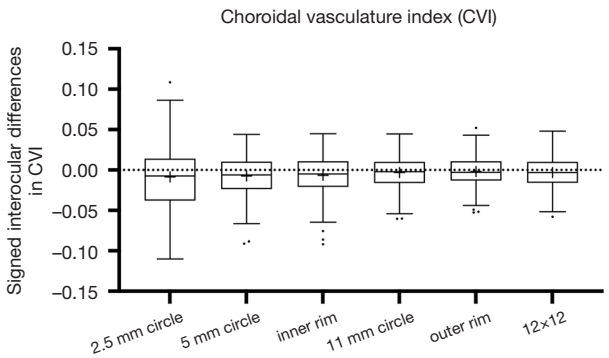

Figure 5 Tukey boxplots of the signed interocular difference of CVI from all 122 participants. Boxplots show the mean as "+". The perforated line indicates the zero. A trend for right eyes to have lower CVIs (the mean value less than 0) shown in the 2.5 mm circle, 5 mm circle, inner rim, 11 mm circle, outer rim and entire 12×12 mm scan regions. CVI, choroidal vascularity index.

Table 5 Correlation coefficients between MCT and CVI in interocular differences

Region quantified	Correlation between MCT and CVI in signed interocular differences (right eye - left eye)		Correlation between MCT and CVI in absolute interocular differences	
	Coefficients	P value	Coefficients	P value
2.5 mm circle	–0.21	0.020	0.01	0.883
5 mm circle	–0.12	0.191	–0.05	0.601
Inner rim	–0.07	0.457	–0.09	0.322
11 mm circle	–0.09	0.349	–0.06	0.531
Outer rim	–0.01	0.878	0.007	0.937
12×12	–0.08	0.369	–0.004	0.967

MCT, mean choroidal thickness; CVI, choroidal vascularity index.

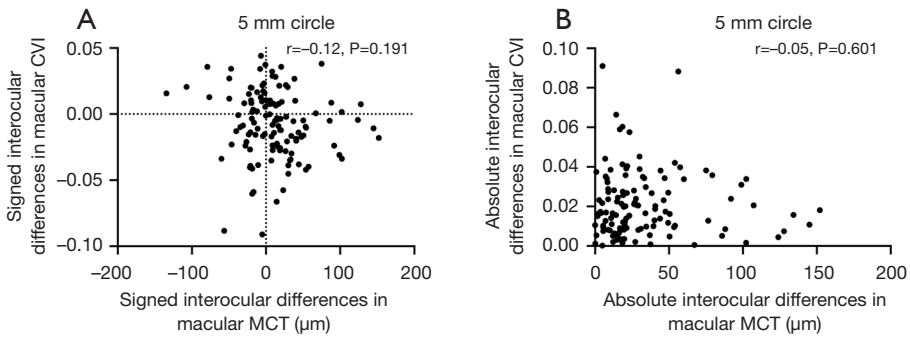

Figure 6 Scatter plots showing relationships between interocular differences in MCT and CVI measurements from all 122 participants in the 5 mm circle (macular) region. (A) The relationship between signed interocular differences in MCT and CVI in the 5 mm circle region. (B) The relationship between absolute interocular differences in MCT and CVI in the 5 mm circle region. MCT, mean choroidal thickness; CVI, choroidal vascularity index.

Factors influencing interocular differences in MCT and CVI measurements

The relationship between interocular differences and clinical factors such as age and axial length are shown in *Tables 6*,7 and *Figures 7*,*8*. Neither the signed nor absolute interocular differences of MCT were significantly related to age or the respective interocular differences in the axial length. Despite a handful of statistically significant correlations between signed interocular difference of CVI and age, none rose to the level of being clinically significant. Therefore, like MCT, the signed or absolute interocular differences of CVI were not significantly related to age or the interocular differences in the axial length.

Discussion

Choroidal diseases can be unilateral, bilateral, or present unilaterally at first, but then progress bilaterally, such as tumors (25), age-related macular degeneration (AMD) (26,27), and polypoidal choroidal vasculopathy (PCV) (28,29). In eyes that appear normal, the appearance of bilateral differences in choroidal measurements between fellow eyes that exceed the range of physiological asymmetry may be the first clue of an evolving pathological process that warrants further examination and follow-up. Therefore, establishing baseline choroidal asymmetry between fellow eyes in the normal population may be of clinical benefit, especially when monitoring for the onset of diseases that tend to affect both eyes.

As expected, our study demonstrated strong correlation of MCT measurements between the right and left eyes in all the regions in this normal population (*Table 2* and *Figure 3*), which is consistent with previous studies (11,12,14,15). Despite a strong correlation of the choroidal thickness

Table 6 Assessment of age influencing interocular differences in MCT and CVI (correlation coefficients, P values)

Measurement	Region quantified	Signed differences	Absolute value differences
MCT	2.5 mm circle	r=–0.08, P=0.375	r=–0.01, P=0.922
	5 mm circle	r=–0.08, P=0.393	r=0.07, P=0.467
	Inner rim	r=–0.10, P=0.297	r=0.07, P=0.472
	11 mm circle	r=0.01, P= 0.945	r=0.16, P=0.070
	Outer rim	r=0.07, P=0.428	r=0.14, P=0.114
	12×12	r=0.003, P=0.972	r=0.18, P=0.046*
CVI	2.5 mm circle	r=0.14, P=0.116	r=0.01, P=0.919
	5 mm circle	r=0.15, P=0.105	r=–0.04, P=0.660
	Inner rim	r=0.12, P=0.204	r=–0.04, P=0.648
	11 mm circle	r=0.19, P=0.037*	r=–0.10, P=0.252
	Outer rim	r=0.20, P=0.030*	r=–0.09, P=0.318
	12×12	r=0.19, P=0.035*	r=–0.16, P=0.084

*, P<0.05. MCT, mean choroidal thickness; CVI, choroidal vascularity index.

Table 7 Assessment of interocular differences in axial length influencing interocular differences in MCT and CVI (correlation coefficients, P values)

Measurement	Region quantified	Signed differences	Absolute value differences
MCT	2.5 mm circle	r=–0.04, P=0.628	r=0.13, P=0.154
	5 mm circle	r=–0.03, P=0.717	r=0.12, P=0.177
	Inner rim	r=–0.03, P=0.780	r=0.11, P=0.234
	11 mm circle	r=0.02, P= 0.791	r=0.16, P=0.080
	Outer rim	r=0.05, P=0.595	r=0.12, P=0.179
	12×12	r=0.01, P=0.893	r=0.16, P=0.080
CVI	2.5 mm circle	r=–0.04, P=0.633	r=–0.03, P=0.742
	5 mm circle	r=–0.05, P=0.610	r=–0.08, P=0.378
	Inner rim	r=–0.03, P=0.705	r=–0.002, P=0.979
	11 mm circle	r=–0.14, P=0.116	r=–0.0002, P=0.999
	Outer rim	r=–0.15, P=0.091	r=0.06, P=0.512
	12×12	r=–0.12, P=0.171	r=0.01, P=0.871

MCT, mean choroidal thickness; CVI, choroidal vascularity.

between fellow eyes, comparison analysis revealed that choroidal thickness in some macular subregions in right eyes tended to be thicker than that in left eyes in normal eyes (8,10,12,15,30). However, two prior studies reported an opposite result, that is, the subfoveal choroidal thickness of the right eyes was thinner compared to the left eyes (11,14). It is worth noting that the results of these prior studies were all derived from manual measurements of selected B-scans, therefore, the subjective bias of the choroidal thickness measurements might lead to discrepancies among studies. Here we showed a significantly thicker MCT in right eyes than in left eyes in all the regions (*Table 2* and *Figure 4*). It is suspected that the interocular choroidal asymmetry of MCT might be attributed to asymmetrical choroidal

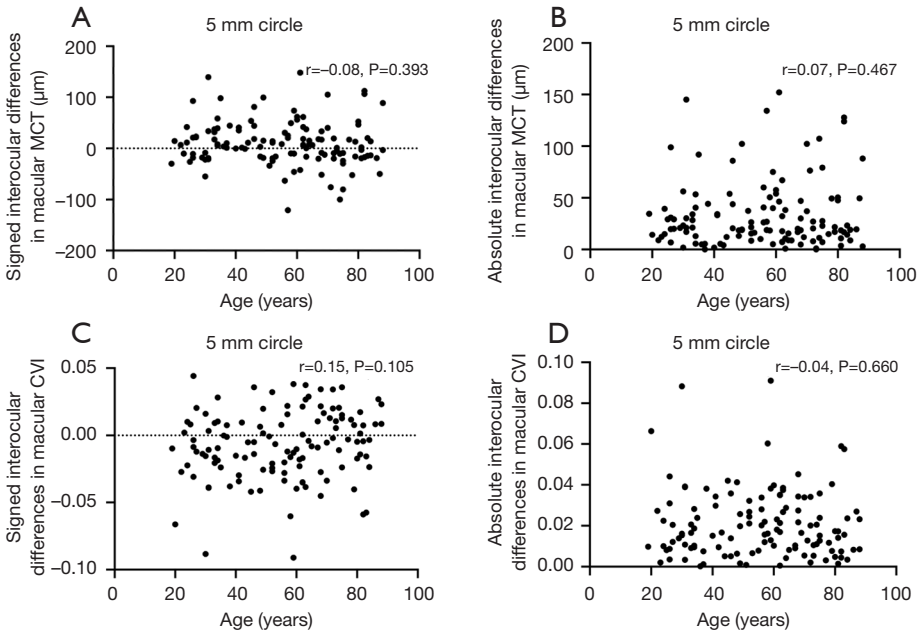

Figure 7 Scatterplots showing relationships between interocular difference in the 5 mm circle (macular) region and age. (A) The relationship between the signed interocular difference in MCT and age. (B) The relationship between the absolute interocular difference in MCT and age. (C) The relationship between the signed interocular difference in CVI measurements and age. (D) The relationship between the absolute interocular difference in CVI and age. MCT, mean choroidal thickness; CVI, choroidal vascularity index.

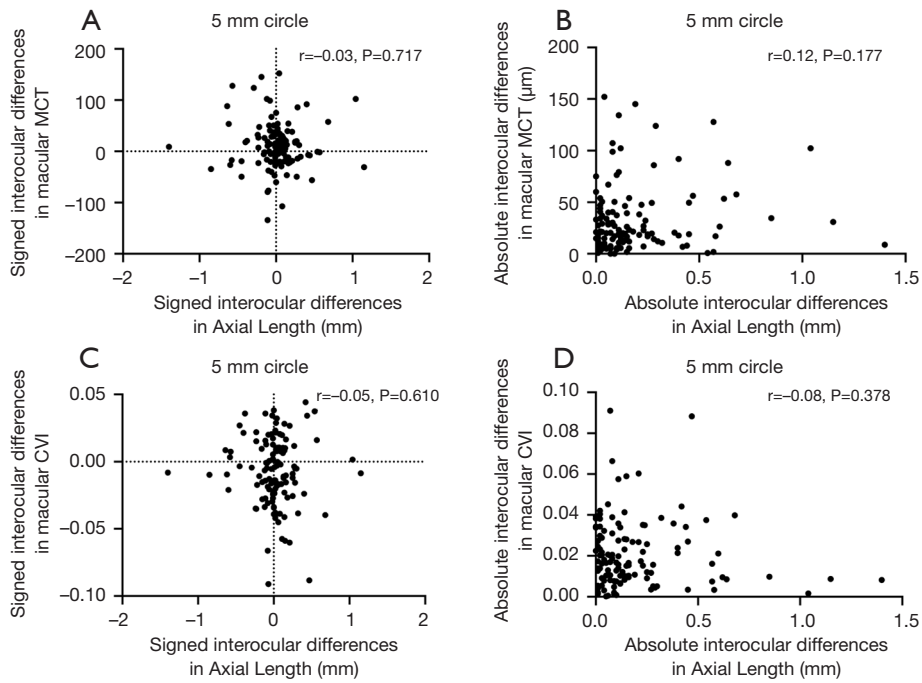

Figure 8 Scatterplots showing relationships between interocular difference in the 5 mm circle (macular) region and axial length. (A) The relationship between the signed interocular difference in MCT and axial length. (B) The relationship between the absolute interocular difference in MCT and axial length. (C) The relationship between the signed interocular difference in CVI measurements and axial length. (D) The relationship between the absolute interocular difference in CVI measurements and axial length. MCT, mean choroidal thickness; CVI, choroidal vascularity index.

blood flow (31-33). One possible explanation of this is the anatomical asymmetry of the aortic arch and common carotid arteries. It is known that the right common carotid originates from the neck from the brachiocephalic trunk, while the left originates in the thorax from the aorta (34), and the choroidal vasculature is supplied by the long and short posterior ciliary and the anterior ciliary arteries (35), all of which are the distal branches of the ophthalmic artery, which arises from the internal carotid artery. The asymmetry of the common carotid arteries, along with variations in vessel curvature, result in hemodynamic differences that may cause observable interocular differences in MCT (34,36). Anatomical asymmetries in non-pathologic choroidal venous drainage (37,38) and autonomic and sensory neural innervation (39) may also precipitate variations in MCT measurements resulting from differences in the choroidal circulation. The vasculature is complicated further by the presence of collateral blood flow from the external carotid arteries (40,41). One future strategy to investigate the asymmetries in choroidal blood flow resulting from interocular variations in anatomic vasculature or neural innervation would be to visualize facial blood flow in relation to asymmetrical choroidal thickness (42). Another possibility is that MCT asymmetry between eyes may be due to eye preference. Previous studies have shown that approximately 70% of the population are right-eye dominant (43,44), and differences linked with eye dominance such as accommodation have been tied to changes in choroidal thickness (45,46). To explore this possibility, we propose that future studies designed to study these interocular choroidal differences will need to document the dominant eye for each subject.

The interocular symmetry in CVI has not been previously studied in detail. We found that unlike a strong interocular correlation in MCT, there was only a moderate interocular correlation in CVI within all corresponding regions (*Table 2*). Our study showed a significantly smaller CVI in the right eyes compared with the left eyes within the central regions (2.5-mm circle, 5-mm circle, 5-mm rim). However, it is worth noting that the size of signed interocular differences in CVI, being only ~0.32% to 1.40% (*Table 4* and *Figure 5*), was very small, therefore, the difference in CVI measurements between fellow eyes is not likely to be clinically significant in normal eyes. In addition, compared with previous methods for measuring CVI on two-dimensional images (i.e., B-scan or *en face* images) (47-49), our method of calculating CVI was performed on the entire volumetric scan, which is thought to be more relevant and reasonable.

In the correlation analysis (*Table 5* and *Figure 6*), neither signed nor absolute interocular differences in MCT were correlated with corresponding CVI interocular differences, which suggests that any mechanism explaining MCT asymmetry may not be what drives the CVI asymmetry. In addition, we did not find any significant correlation between the interocular differences (including both signed and absolute differences) in MCT and CVI measurements and the age of the participants (*Table 6*), indicating that age-specific normal ranges for MCT and CVI symmetry measurements are not necessary. Although Chen *et al.* (12) reported a marginally significant trend (r=–0.20, P=0.048) for reduced absolute differences in foveal choroidal thickness with the increase of age, the degree of the relationship did not rise to the level of being clinically significant. Signed interocular MCT differences also showed no relationship with signed interocular axial length differences (*Figure 8*), which was inconsistent with the result reported by Kim *et al.* (15) in which the interocular choroidal thickness and axial length differences had a significant negative correlation. This may be due to the differences in the measurement methods used and the distribution of participants' age between these two studies, as well as the exclusion of participants with axial lengths greater than 26-mm axial length in our study.

While promising, there were some notable limitations in this study. Firstly, we did not acquire other information (e.g., dominant eye, interocular pressure, visual acuity, and refraction errors) that may influence interocular choroidal symmetry. While we excluded eyes with pathological myopia, myopia has been correlated with increased interocular differences in choroidal thickness with thinning of choroid in the more myopic eye (50-53). Characterizing atypical MCT in cases of asymmetric myopia would further refine a clinical baseline for physiologic asymmetries in MCT, as well as pathologies linked to eyes with greater degrees of myopia (54). However, given that our intention was primarily to assess the physiological choroidal asymmetry in MCT and CVI within normal eyes, this limitation was not thought to diminish the validity of this study. Secondly, our study was a cross-sectional study and only involved one time point, which may result in inclusion of participants whose ocular diseases were at a very early stage and did not meet clinical diagnostic criteria. This is a common limitation for all current studies investigating interocular asymmetry of the choroid in normal eyes (8,10-12,15,55). Future studies will need to recruit more

participants and carry out multiple clinical examinations and SS-OCT imaging sessions to distinguish participants who currently appear "normal" but later develop ocular diseases, such as AMD.

To the best of our knowledge, we are unaware of any report using widefield SS-OCT imaging to investigate choroidal symmetry between fellow normal eyes. Our study has successfully demonstrated subtle differences in MCT and CVI measurements between fellow normal eyes using SS-OCT and established 95% normal limits for these measurements between eyes. This study will be useful clinically in assisting clinicians and researchers in distinguishing pathological eyes from eyes that are within the tolerance limits for physiological asymmetry.

Acknowledgments

Funding: Research supported by grants from the National Eye Institute (R01EY028753), the Salah Foundation, Carl Zeiss Meditec, an unrestricted grant from the Research to Prevent Blindness, Inc., New York, NY, USA and the National Eye Institute Center Core Grant (P30EY014801) to the Department of Ophthalmology, University of Miami Miller School of Medicine. The funding organization had no role in the design or conduct of this research.

Footnote

Reporting Checklist: The authors have completed the STROBE reporting checklist. Available at https://dx.doi.org/10.21037/qims-21-813

Conflicts of Interest: All authors have completed the ICMJE uniform disclosure form (available at https://dx.doi.org/10.21037/qims-21-813). GG, PJR and RKW received research support from Carl Zeiss Meditec, Inc. Giovanni Gregori and the University of Miami co-own a patent that is licensed to Carl Zeiss Meditec, Inc. PJR also received research funding from Stealth BioTherapeutics. He is also a consultant for Apellis, Bayer, Boehringer-Ingelheim, Carl Zeiss Meditec, Chengdu Kanghong Biotech, InflammX Therapeutics, Ocudyne, Regeneron Pharmaceuticals, and Unity Biotechnology. He also has equity interest in Apellis, Valitor Verana Health, and Ocudyne. RKW disclosured intellectual property owned by the Oregon Health and Science University and the University of Washington. Dr. RKW also received research support from Moptim Inc., Colgate Palmolive Company and Facebook technologies LLC. He is a consultant for Carl Zeiss Meditec, Cyberdontics, Optos. RKW serves as an unpaid Deputy Editor of *Quantitative Imaging in Medicine and Surgery*. Mr. JC is a medical research Intern at the University of Washington during this research. He is currently pursuing a medical degree at Washington State University Elson S. Floyd College of Medicine. The other authors have no conflicts of interest to declare.

Ethical Statement: The authors are accountable for all aspects of the work in ensuring that questions related to the accuracy or integrity of any part of the work are appropriately investigated and resolved. This study was approved by the Institutional Review Board (IRB) of Medical Sciences Subcommittee at the University of Miami, Miller School of Medicine and was conducted in compliance with the Declaration of Helsinki (as revised in 2013). All participants voluntarily gave written informed consents before scans were taken.

References

1. Huynh SC, Wang XY, Burlutsky G, Mitchell P. Symmetry of optical coherence tomography retinal measurements in young children. Am J Ophthalmol 2007;143:518-20.
2. Al-Haddad C, Antonios R, Tamim H, Noureddin B. Interocular symmetry in retinal and optic nerve parameters in children as measured by spectral domain optical coherence tomography. Br J Ophthalmol 2014;98:502-6.
3. Liu G, Keyal K, Wang F. Interocular Symmetry of Vascular Density and Association with Central Macular Thickness of Healthy Adults by Optical Coherence Tomography Angiography. Sci Rep 2017;7:16297.
4. Hou H, Moghimi S, Zangwill LM, Shoji T, Ghahari E, Manalastas PIC, Penteado RC, Weinreb RN. Inter-eye Asymmetry of Optical Coherence Tomography Angiography Vessel Density in Bilateral Glaucoma, Glaucoma Suspect, and Healthy Eyes. Am J Ophthalmol

2018;190:69-77.
5. Kanellopoulos AJ, Chiridou M, Asimellis G. Optical coherence tomography-derived corneal thickness asymmetry indices: clinical reference study of normal eyes. J Cataract Refract Surg 2014;40:1603-9.
6. Mahmudi T, Kafieh R, Rabbani H, Mehri A, Akhlaghi MR. Evaluation of Asymmetry in Right and Left Eyes of Normal Individuals Using Extracted Features from Optical Coherence Tomography and Fundus Images. J Med Signals Sens 2021;11:12-23.
7. Park JJ, Oh DR, Hong SP, Lee KW. Asymmetry analysis of the retinal nerve fiber layer thickness in normal eyes using optical coherence tomography. Korean J Ophthalmol 2005;19:281-7.
8. Ruiz-Medrano J, Flores-Moreno I, Peña-García P, Montero JA, Duker JS, Ruiz-Moreno JM. Asymmetry in macular choroidal thickness profile between both eyes in a healthy population measured by swept-source optical coherence tomography. Retina 2015;35:2067-73.
9. Miller AR, Roisman L, Zhang Q, Zheng F, Rafael de Oliveira Dias J, Yehoshua Z, Schaal KB, Feuer W, Gregori G, Chu Z, Chen CL, Kubach S, An L, Stetson PF, Durbin MK, Wang RK, Rosenfeld PJ. Comparison Between Spectral-Domain and Swept-Source Optical Coherence Tomography Angiographic Imaging of Choroidal Neovascularization. Invest Ophthalmol Vis Sci 2017;58:1499-505.
10. Al-Haddad C, El Chaar L, Antonios R, El-Dairi M, Noureddin B. Interocular symmetry in macular choroidal thickness in children. J Ophthalmol 2014;2014:472391.
11. Orduna E, Sanchez-Cano A, Luesma MJ, Perez-Navarro I, Abecia E, Pinilla I. Interocular Symmetry of Choroidal Thickness and Volume in Healthy Eyes on Optical Coherence Tomography. Ophthalmic Res 2018;59:81-7.
12. Chen FK, Yeoh J, Rahman W, Patel PJ, Tufail A, Da Cruz L. Topographic variation and interocular symmetry of macular choroidal thickness using enhanced depth imaging optical coherence tomography. Invest Ophthalmol Vis Sci 2012;53:975-85.
13. Kang HM, Kim SJ, Koh HJ, Lee CS, Lee SC. Discrepancy in Subfoveal Choroidal Thickness in Healthy Adults with Isometropia. Ophthalmology 2015;122:2363-4.
14. Spaide RF, Koizumi H, Pozzoni MC. Enhanced depth imaging spectral-domain optical coherence tomography. Am J Ophthalmol 2008;146:496-500.
15. Kim MS, Lim HB, Lee WH, Kim KM, Nam KY, Kim JY. Wide-Field Swept-Source Optical Coherence Tomography Analysis of Interocular Symmetry of Choroidal Thickness in Healthy Young Individuals. Invest Ophthalmol Vis Sci 2021;62:5.
16. Zhou H, Dai Y, Shi Y, Russell JF, Lyu C, Noorikolouri J, Feuer WJ, Chu Z, Zhang Q, de Sisternes L, Durbin MK, Gregori G, Rosenfeld PJ, Wang RK. Age-Related Changes in Choroidal Thickness and the Volume of Vessels and Stroma Using Swept-Source OCT and Fully Automated Algorithms. Ophthalmol Retina 2020;4:204-15.
17. Zhou H, Chu Z, Zhang Q, Dai Y, Gregori G, Rosenfeld PJ, Wang RK. Attenuation correction assisted automatic segmentation for assessing choroidal thickness and vasculature with swept-source OCT. Biomed Opt Express 2018;9:6067-80.
18. Yiu G, Pecen P, Sarin N, Chiu SJ, Farsiu S, Mruthyunjaya P, Toth CA. Characterization of the choroid-scleral junction and suprachoroidal layer in healthy individuals on enhanced-depth imaging optical coherence tomography. JAMA Ophthalmol 2014;132:174-81.
19. Vermeer KA, Mo J, Weda JJ, Lemij HG, de Boer JF. Depth-resolved model-based reconstruction of attenuation coefficients in optical coherence tomography. Biomed Opt Express 2013;5:322-37.
20. Kirby MA, Li C, Choi WJ, Gregori G, Rosenfeld P, Wang R. Why choroid vessels appear dark in clinical OCT images. Available online: https://www.spiedigitallibrary.org/conference-proceedings-of-spie/10474/1047428/Why-choroid-vessels-appear-dark-in-clinical-OCT-images/10.1117/12.2291057.short?SSO=1
21. Wang RK, Kirby M, Li C, Choi WJ, Gregori G, Rosenfeld PJ. An explanation for why choroidal blood vessels appear dark on clinical OCT images. Invest Ophthalmol Vis Sci 2017;58:4754.
22. Chen CL, Wang RK. Optical coherence tomography based angiography Invited. Biomed Opt Express 2017;8:1056-82.
23. Otsu N. A threshold selection method from gray-level histograms. Available online: https://ieeexplore.ieee.org/document/4310076
24. Fleiss JL. The design and analysis of clinical experiments. New York, NY: John Wiley & Sons, 1986:1-6.
25. Say EA, Shah SU, Ferenczy S, Shields CL. Optical coherence tomography of retinal and choroidal tumors. J Ophthalmol 2012;2012:385058.
26. Joachim N, Colijn JM, Kifley A, Lee KE, Buitendijk GHS, Klein BEK, Myers CE, Meuer SM, Tan AG, Holliday EG, Attia J, Liew G, Iyengar SK, de Jong PTVM, Hofman A, Vingerling JR, Mitchell P, Klaver CCW, Klein R, Wang JJ. Five-year progression of unilateral age-related

macular degeneration to bilateral involvement: the Three Continent AMD Consortium report. Br J Ophthalmol 2017;101:1185-92.
27. Gattoussi S, Cougnard-Grégoire A, Korobelnik JF, Rougier MB, Delyfer MN, Schweitzer C, Le Goff M, Merle BMJ, Dartigues JF, Delcourt C. CHOROIDAL THICKNESS, VASCULAR FACTORS, AND AGE-RELATED MACULAR DEGENERATION: The ALIENOR Study. Retina 2019;39:34-43.
28. Fan D, Hua R. Different imaging characteristics between unilateral and bilateral polypoidal choroidal vasculopathy. Photodiagnosis Photodyn Ther 2019;26:1-7.
29. Scassellati-Sforzolini B, Mariotti C, Bryan R, Yannuzzi LA, Giuliani M, Giovannini A. Polypoidal choroidal vasculopathy in Italy. Retina 2001;21:121-5.
30. Bhayana AA, Kumawat D, Kumar V, Chandra M, Chandra P, Sihota R, Kumar A. Interocular asymmetry in choroidal thickness in healthy Indian population using swept-source optical coherence tomography. Indian J Ophthalmol 2019;67:1252-3.
31. Vance SK, Imamura Y, Freund KB. The effects of sildenafil citrate on choroidal thickness as determined by enhanced depth imaging optical coherence tomography. Retina 2011;31:332-5.
32. Kim DY, Silverman RH, Chan RV, Khanifar AA, Rondeau M, Lloyd H, Schlegel P, Coleman DJ. Measurement of choroidal perfusion and thickness following systemic sildenafil (Viagra(®)). Acta Ophthalmol 2013;91:183-8.
33. Kubota T, Jonas JB, Naumann GO. Decreased choroidal thickness in eyes with secondary angle closure glaucoma. An aetiological factor for deep retinal changes in glaucoma? Br J Ophthalmol 1993;77:430-2.
34. Manbachi A, Hoi Y, Wasserman BA, Lakatta EG, Steinman DA. On the shape of the common carotid artery with implications for blood velocity profiles. Physiol Meas 2011;32:1885-97.
35. Zeiss CJ, Tu DC, Phan I, Wong R, Treuting PM. 21 - Special Senses: Eye. In: Treuting PM, Dintzis SM, Montine KS, editors. Comparative Anatomy and Histology. Second edition. San Diego: Academic Press, 2018:445-70.
36. Wenn CM, Newman DL. Arterial tortuosity. Australas Phys Eng Sci Med 1990;13:67-70.
37. Kutoglu T, Yalcin B, Kocabiyik N, Ozan H. Vortex veins: anatomic investigations on human eyes. Clin Anat 2005;18:269-73.
38. Hiroe T, Kishi S. Dilatation of Asymmetric Vortex Vein in Central Serous Chorioretinopathy. Ophthalmol Retina 2018;2:152-61.
39. Reiner A, Fitzgerald MEC, Del Mar N, Li C. Neural control of choroidal blood flow. Prog Retin Eye Res 2018;64:96-130.
40. Van Allen MW, Blodi FC. Collateral circulation to the eye in occlusion of the internal carotid artery; observations on the influence of external carotid flow on retinal artery pressure. Arch Neurol 1960;2:74-8.
41. Tamler E, Takahashi E. Collateral circulation to the eye. Am J Ophthalmol 1961;52:381-4.
42. Xie Z, Wang G, Cheng Y, Zhang Q, Le MN, Wang RK. Optical coherence tomography angiography measures blood pulsatile waveforms at variable tissue depths. Quant Imaging Med Surg 2021;11:907-17.
43. Eser I, Durrie DS, Schwendeman F, Stahl JE. Association between ocular dominance and refraction. J Refract Surg 2008;24:685-9.
44. Ehrenstein WH, Arnold-Schulz-Gahmen BE, Jaschinski W. Eye preference within the context of binocular functions. Graefes Arch Clin Exp Ophthalmol 2005;243:926-32.
45. Woodman-Pieterse EC, Read SA, Collins MJ, Alonso-Caneiro D. Regional Changes in Choroidal Thickness Associated With Accommodation. Invest Ophthalmol Vis Sci 2015;56:6414-22.
46. Fujimura F, Handa T, Kawamorita T, Shoji N. The effect of ocular dominance on accommodation and miosis under binocular open viewing conditions. Open J Ophthalmol 2017;7:158-66.
47. Zheng F, Gregori G, Schaal KB, Legarreta AD, Miller AR, Roisman L, Feuer WJ, Rosenfeld PJ. Choroidal Thickness and Choroidal Vessel Density in Nonexudative Age-Related Macular Degeneration Using Swept-Source Optical Coherence Tomography Imaging. Invest Ophthalmol Vis Sci 2016;57:6256-64.
48. Agrawal R, Gupta P, Tan KA, Cheung CM, Wong TY, Cheng CY. Choroidal vascularity index as a measure of vascular status of the choroid: Measurements in healthy eyes from a population-based study. Sci Rep 2016;6:21090.
49. Iovino C, Pellegrini M, Bernabei F, Borrelli E, Sacconi R, Govetto A, Vagge A, Di Zazzo A, Forlini M, Finocchio L, Carnevali A, Triolo G, Giannaccare G. Choroidal Vascularity Index: An In-Depth Analysis of This Novel Optical Coherence Tomography Parameter. J Clin Med 2020;9:595.
50. Alzaben Z, Cardona G, Zapata MA, Zaben A. Interocular asymmetry in choroidal thickness and retinal sensitivity in high myopia. Retina 2018;38:1620-8.

51. Vincent SJ, Collins MJ, Read SA, Carney LG. Retinal and choroidal thickness in myopic anisometropia. Invest Ophthalmol Vis Sci 2013;54:2445-56.
52. Harb E, Hyman L, Gwiazda J, Marsh-Tootle W, Zhang Q, Hou W, Norton TT, Weise K, Dirkes K, Zangwill LM; COMET Study Group. Choroidal Thickness Profiles in Myopic Eyes of Young Adults in the Correction of Myopia Evaluation Trial Cohort. Am J Ophthalmol 2015;160:62-71.e2.
53. Shao L, Xu L, Wei WB, Chen CX, Du KF, Li XP, Yang M, Wang YX, You QS, Jonas JB. Visual acuity and subfoveal choroidal thickness: the Beijing Eye Study. Am J Ophthalmol 2014;158:702-709.e1.
54. Breher K, Ohlendorf A, Wahl S. Myopia induces meridional growth asymmetry of the retina: a pilot study using wide-field swept-source OCT. Sci Rep 2020;10:10886.
55. Yang M, Wang W, Xu Q, Tan S, Wei S. Interocular symmetry of the peripapillary choroidal thickness and retinal nerve fibre layer thickness in healthy adults with isometropia. BMC Ophthalmol 2016;16:182.

Cite this article as: Lu J, Zhou H, Shi Y, Choe J, Shen M, Wang L, Chen K, Zhang Q, Feuer WJ, Gregori G, Rosenfeld PJ, Wang RK. Interocular asymmetry of choroidal thickness and vascularity index measurements in normal eyes assessed by swept-source optical coherence tomography. Quant Imaging Med Surg 2022;12(1):781-795. doi: 10.21037/qims-21-813

